

Enhancement of ciprofloxacin removal by modifying activated carbon (AC-S) derived from corn stalks with novel silage pre-treatment

Daoji Wu^{a,b}, Chenxi Nie^{a,c}, Jingtao Xu^{a,b,*}, Congcong Zhao^{d,*}, Fengxun Tan^a, Xiaomei Sun^e, Yuming Jing^f, Ning Wang^a, Wenjun Yin^a, Guocun Ding^a, Bing Xu^a

^aSchool of Municipal and Environmental Engineering, Shandong Jianzhu University, Jinan 250101, China, email: tfx@sdjzu.edu.cn; xubing1977@sdjzu.edu.cn

^bCo-Innovation Center of Green Building, Shandong, Jinan 250101, China, email: xujingtiao@sdjzu.edu.cn, wdj@sdjzu.edu.cn

^cJinan Water Group Co. Ltd., Jinan 250012, China, email: niechenxi123@163.com

^dKey Laboratory of Colloid and Interface Chemistry, Shandong University, Jinan 250100, China, email: zhaocongcong1009@163.com

^eShandong Sanrun Environmental Protection Science Co. Ltd., Shandong, Jinan 250101, China, email: 275108319@qq.com

^fShandong Academy of Environmental Science, Environmental Engineering Co. Ltd., Shandong, Jinan 250101, China, email: jingym08@163.com

Received 9 January 2017; Accepted 27 July 2017

ABSTRACT

Ciprofloxacin (CIP), a common antibiotic, is widely detected in wastewater and soil. This study proposes a novel method for preparing activated carbon with corn stalks pre-treated with silage (AC-S). This study examined physical characteristics of activated carbons with N₂ adsorption/desorption, scanning electron microscopy, X-ray diffraction, Fourier transform infrared spectroscopy (FTIR), and Boehm titration. Adsorption of CIP was enhanced by activated carbon. Laboratory experiments were conducted to investigate adsorption kinetics, equilibrium isotherms, and influence of chemical characteristics of solution (i.e., pH and ionic strength). Both kinds of activated carbon-prepared with corn stalks (AC) and AC-S featured surface areas of more than 700 m²/g. Although total pore volume of AC (1.178 cm³/g) was higher than that of AC-S (0.4681 cm³/g), microspore proportion of AC-S reached 60%, which was considerably higher compared with that of AC (24%). AC-S exhibited a faster increasing rate in a portion of microspore surface area than AC. FTIR and Boehm titration indicated that AC-S contained higher amounts of surface-acidic functional groups, namely, carboxyl, phenolic, and hydroxyl. Adsorption experiments agreed well with pseudo-second-order and Langmuir models. Maximum adsorption capacity of CIP on AC-S reached 407.75 mg/g, which was 26.2% higher than that of AC. Results showed that possible mechanisms for CIP adsorption on AC-S may include hydrophobic interaction, chemical adsorption, electrostatic attraction, and π - π EDA interaction.

Keywords: Activated carbon; Adsorption; Ciprofloxacin; Corn stalk; Silage pretreatment

1. Introduction

Antibiotics are routinely administered to animals and humans to protect them against bacterial infections; they were recently recognized as emerging environmental contaminants [1]. A typical antibiotic, Ciprofloxacin (CIP) is a fluoroquinolone class antibiotic with broad-spectrum antibacterial activity and satisfactory sterilizing effect [2]. As CIP cannot be thoroughly adsorbed and metabolized by

the human body, most residues are discharged into sewage systems by excretion [1]. To date, CIP is widely detected in coastal areas [3], soil [4], wastewater, and underground and surface waters [5]. According to Peng et al. [6], around 22 tons of fluoroquinolone entered wastewater via sludge in Guangzhou in 2007. CIP concentration reached between 0.007 and 0.002 nmol/g in two marine aquaculture areas of the Pearl River Delta [3], and its maximum concentration measured 0.20 nmol/L in marine waters of a coast in China [7]. Accumulation of CIP in the environment can produce antibiotic resistant bacteria, which may result in hard-to-treat diseases and potential risks to human health and ecosystem [8].

*Corresponding author.

Adsorption is a common and effective method for eliminating CIP from wastewater. Among commercial adsorbents, activated carbon is one of the most widely used in wastewater treatment plants due to its high adsorption capacity and low cost. Numerous references reported adsorption of CIP by activated carbon and preparation of activated carbon using date palm leaflets [9], specific bamboos [10], and wetland plants, such as *Cyperus alternifolius* [11]. However, few studies were conducted on the use of activated carbon prepared from corn stalks (AC) to adsorb CIP. Adding modifiers, such as urea [12], guanidine phosphate [13], and organic acids [14], is a popular way for improving adsorption capacity of activated carbon. However, such addition can increase cost of preparation and result in production of pollutants during modification. Therefore, studies should develop an environment-friendly and cost-effective modification method.

Corn is one of the most important crops in the world, particularly in China [15]. Annual worldwide production of corn approximately reaches 520 million tons [16]. However, corn stalks are usually left in fields after harvest without utilization. In China, most corn stalks are burnt in situ, causing severe air pollution. Some researchers once used corn stalks and corn cob with H_3PO_4 or acrylic as modifier to prepare activated carbon; the prepared activated carbon can effectively remove heavy metals, such as chromium and cadmium, with a removal rate of 16.0%–99.2% [17,18]. AC can also effectively remove Direct Red 23 [19]. Therefore, as a raw material for activated carbon, corn stalks can provide an alternative recycling method and reduce air pollution to some extent [20]. A previous study [21] demonstrated that owing to its high nutritional content, corn stalks can be used in preparing silage to feed animals. Silage was also applied in biogas production. For example, researchers [22, 23] studied effects of trace elements on biogas production based on a model substrate for maize silage. Silage is an ideal way of improving rate of corn stalks usage. Ensiling features many advantages, including low-cost production, long-term storage, and ease of operation. Some acidic functional groups can also be produced during ensiling, which can enrich such groups on surfaces of prepared activated carbon. Therefore, silage-activated carbon not only improves usage of biological straw in a low-cost manner but also promotes environmental protection. Nevertheless, at present, using corn stalks with silage pre-treatment (AC-S) is hardly considered in production of activated carbon.

This study aims to introduce the use of AC-S as raw material in producing activated carbon. Performed evaluations determined characteristics of activated carbon and adsorption capability of CIP in terms of kinetics and equilibrium. This paper provides a novel method for preparation of activated carbon and improved utilization ratio of corn stalks. As a new approach which does not require addition of chemical modification agents, the proposed method can save energy and is cost-effective; these properties bear significance in preventing environmental pollution by antibiotics.

2. Materials and methods

2.1. Materials

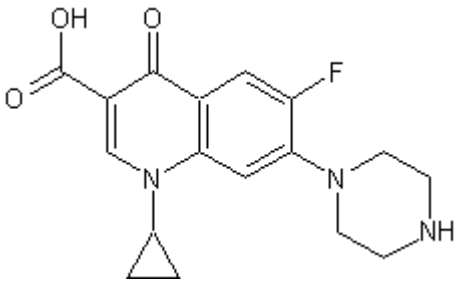
Chemical reagents used in experiments were of analytical grade. CIP hydrochloride (purity of 97.5%–102.0%) was supplied by Sangon Biotech (Shanghai, China); its characteristics are listed in Table 1. All solutions were prepared by suitable dilution with deionized water.

2.2. Activated carbon preparation

Corn stalks were obtained from Anjia Farmland in Jinan, Shandong Province. Corn stalks were cut into 20–30 mm pieces with moisture content of 45%–60%. Half of corn stalks were dried, whereas the rest were used for silage. Processing methods, which include chopping, compacting, and sealing, can improve silage quality [22]. AC-S were mounted directly in a silage jar then compacted. Sealed with mud, the silage jar was stored in the dark at 15–20°C for fermentation. After 20 d, the silage jar was opened and checked to determine whether corn stalks developed the following characteristics: yellow and green, soft and slightly wet, and smelled the same as alcohol. When these characteristics were confirmed, then silage process was considered successful.

Dried corn stalks and corn stalk silage were both ground and sieved into particles with sizes of 15 and 30 mm, respectively. Samples were soaked in 85 wt% H_3PO_4 at a mass ratio of 2:1 (H_3PO_4 :Stalks) for 10 h at 20°C. Samples were then carbonized at 450°C for 1 h in a muffle furnace. After cooling at room temperature, carbonized samples were thoroughly washed with deionized water until pH of

Table 1
Main characteristics and structure of CIP

| Name | Molecular formula | Molecular weight | Molecular structure | pK_{a1} | pK_{a2} |
|---------------------|-----------------------|------------------|--|-----------|-----------|
| Ciprofloxacin (CIP) | $C_{17}H_{18}FN_3O_3$ | 331.35 |  | 6.1 | 8.7 |

filtrate was close to neutral. Then, samples were dried for 12 h at 105°C. Finally, AC and AC-S were sorted with standard 160/200 mesh sieves (Model ø200).

2.3. Characterization

Brunauer–Emmett–Teller (BET) surface area and pore structure of the activated carbon were determined by N₂ adsorption–desorption at 77 K using a surface area analyzer (Quantachrome Corporation, USA). Scanning electron microscopy (SEM) (JEOL, JSM-6700F, Japan) was employed to analyze surface morphology of carbon. Fourier transform infrared spectroscopy (FTIR) was determined using a FTIR spectrometer (VERTEX70 spectrometer, Bruker Corporation, Germany) at a wavelength range of 400–4000 cm⁻¹ with background subtraction. Surface functional groups were measured using Boehm titration [24].

Point of zero charge (PZC) was determined as follows [25]: a series of 0.01 M NaCl solutions were adjusted to different pH values (from 2 to 11), as measured by a pH meter (pH S-3C, Shanghai, China), using HCl acid. Then, 0.15 g of dry carbon was placed in 50 mL solutions, and final pH was measured after 48 h of agitation. When addition of samples did not cause changes in pH value, samples were labeled as pH_{pzc}.

2.4. CIP adsorption

For adsorption kinetic experiments, 0.4 g of activated carbon (AC or AC-S) were mixed with CIP (200 mg/L, 1000 mL) in a beaker with initial pH of 6.04. Kinetic properties were studied by measuring contact equilibrium time. Supernatant was filtered and sampled by using 0.45 μm membrane at different time intervals. Adsorption isotherm experiments were performed at 30±1°C with CIP concentration from 100 mg/L to 1000 mg/L. Serial experiments were performed by agitating samples (20 mg) in CIP solution (200 mg/L, 50 mL). Effect of pH on CIP removal was studied at pH 2.0–7.0 after adjustment by 0.1 M NaOH and 0.1 M HCl solution. Effect of ionic strength on CIP solutions was evaluated at different ionic strengths (0–0.5 M NaCl) in CIP solution (200 mg/L).

For all experiments, CIP concentration in water samples was determined using a UV-visible spectrophotometer (UV-754, Shanghai) at 275 nm after filtrating through a 0.45 μm membrane. Removal efficiency and adsorption capacity of CIP on activated carbon, Q_e (mg/g), were calculated according to Eqs. (1) and (2), respectively [26,27]:

$$Q_e = \frac{(C_0 - C_e)V}{W} \quad (1)$$

$$\text{Removal efficiency (\%)} = \frac{C_0 - C_e}{C_0} \times 100\% \quad (2)$$

where C_0 and C_e represent the initial and equilibrium concentrations of CIP in aqueous solution (mg/L), respectively; V refers to volume (L) of solution; and W (g) corresponds to mass of adsorbent used.

3. Results and discussion

3.1. Physical characteristics of adsorbents

Pore structure bears significance in adsorption performance of activated carbons. Fig. 1 shows N₂ adsorption and desorption isotherms and pore size distribution of AC and AC-S. For AC, adsorption and desorption isotherms did not overlap but formed a wider hysteresis loop due to capillary condensation. According to classification of adsorption isotherm by IUPAC [28], adsorption isotherm belonged to Type IV, suggesting one or more steps in adsorption isotherms. For AC-S, adsorption type was categorized as monolayer adsorption (I), which was similar to the Langmuir isotherm. As shown in Table 2, BET surface area of AC measured 1091.223 m²/g, which was higher than that of AC-S (741.63 m²/g). However, surface area alone was insufficient for evaluating adsorbents [29,30]. In AC, total pore and micropore volumes totaled 1.178 and 0.283 cm³/g,

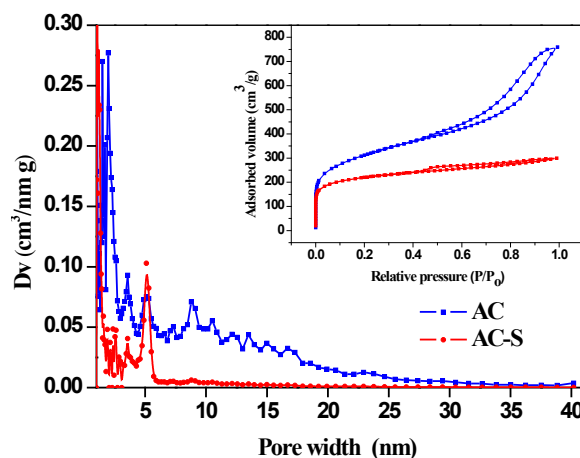


Fig. 1. Pore size distributions (N₂ adsorption/desorption isotherms (inset)) for AC and AC-S.

Table 2
Textural and chemical characteristics of activated carbon

| Activated carbon | AC | AC-S |
|--------------------------------|---------|--------|
| S_{BET} (m ² /g) | 1091.22 | 741.63 |
| S_{mic} (m ² /g) | 583.92 | 579.80 |
| S_{mic}/S_{BET} (%) | 53.5 | 78.2 |
| V_{tot} (cm ³ /g) | 1.178 | 0.468 |
| V_{mic} (cm ³ /g) | 0.283 | 0.281 |
| V_{mic}/V_{tot} (%) | 24.00 | 60.00 |
| D_p (nm) | 4.32 | 2.53 |
| Carboxyl (mmol/g) | 0.636 | 0.914 |
| Lactone (mmol/g) | 0.071 | 0.057 |
| Phenolic (mmol/g) | 1.107 | 1.371 |
| Total acidic (mmol/g) | 1.814 | 2.342 |
| pH _{pzc} | 6.13 | 5.76 |

S_{BET} : BET surface area; S_{ext} : external surface area;
 S_{mic} : micropore surface area; V_{tot} : total pore volume;
 V_{mic} : micropore volume; D_p : the mean pore diameter.

respectively. Meanwhile, in AC-S, total pore and micropore volumes reached $0.4681 \text{ cm}^3/\text{g}$ and $0.281 \text{ cm}^3/\text{g}$, respectively. $S_{\text{mic}}/S_{\text{BET}}$ and $V_{\text{mic}}/V_{\text{tot}}$ values of AC totaled 53.5% and 24%, respectively, which were much lower than those of AC-S (78.2% and 60%), thus indicating that AC-S contained relatively more micropores (0.35–2 nm). Surface functional groups generated by silage pretreatment blocked some macropores in AC-S, thus forming more micropores. This result was confirmed by average pore diameters of two samples; average diameters measured 4.32 and 2.53 nm for AC and AC-S, respectively.

Fig. 2 shows SEM and X-ray diffraction (XRD) patterns of AC and AC-S. AC (Fig. 2a,b) featured a smooth surface, whereas AC-S showed an irregular surface even at higher amplification factors (Fig. 2c,d). SEM images of AC-S illustrated the presence of surface functional groups, which were attached to AC-S in accordance with scanning electron micrographs. XRD patterns of AC and AC-S also differed: AC-S presented fewer prominent peaks, indicating a different crystal structure. The strong peak (2) was due to stacking structure of aromatic layers [31]. AC-S also yielded peaks at 35° , 39.5° , and 40.5° , with intensities higher than those of AC in composites. This result suggested that

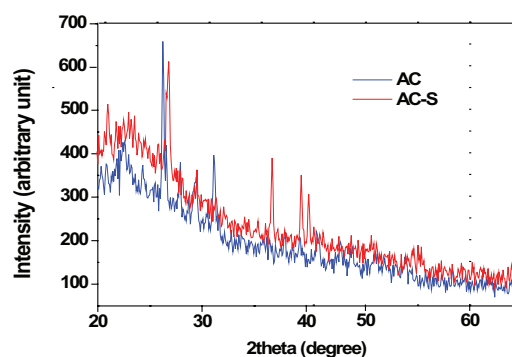
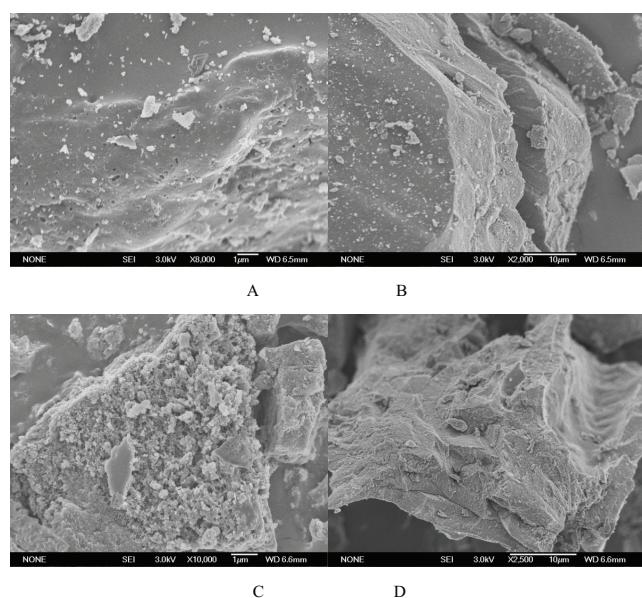


Fig. 2. SEM micrographs of AC (A, B) and AC-S (C, D), and XRD patterns.

crystallite size of AC-S decreased in composites due to silage pretreatment [32].

Fig. 3 shows representative FTIR spectra of AC, AC-S, AC-CIP, and AC-S CIP. Results showed that AC and AC-S shared significantly similar FTIR spectra, suggesting similar functional groups in the two adsorbents. The peak at 3419 cm^{-1} is possibly hydroxyl (–OH) or phenolic hydroxyl absorption peak [33]. Another peak at 1559 cm^{-1} can be attributed to carbonyl (–C=O) double-bond region [34]. As carboxyl vibration was suggested to fall within the range of 1366 cm^{-1} to 1400 cm^{-1} , the amount of carboxyl group significantly increased in AC-S after silage pretreatment [33]. Parts of spectra at 1000 – 1300 cm^{-1} were ascribed to C–O single bonds [35]. Although AC and AC-S both featured the same surface functional groups, AC-S contained more acid groups, coinciding with results of Boehm titration (Table 2). Total acid group of AC-S measured 2.342 mmol/g , which was much higher than that of AC (1.814 mmol/g), especially for carboxyl, which was 1.5 times higher in AC-S (0.914 mmol/g) than in AC. Therefore, silage pretreatment enhanced surface acidity of AC-S. AC-S demonstrated lower transmittance than AC at other wavelengths, suggesting that AC-S contained more surface oxygen-containing functional groups than AC [36].

According to Fig. 4, pH_{pzc} values of AC and AC-S reached 6.13 and 5.76, respectively. When $\text{pH} < \text{pH}_{\text{pzc}}$,

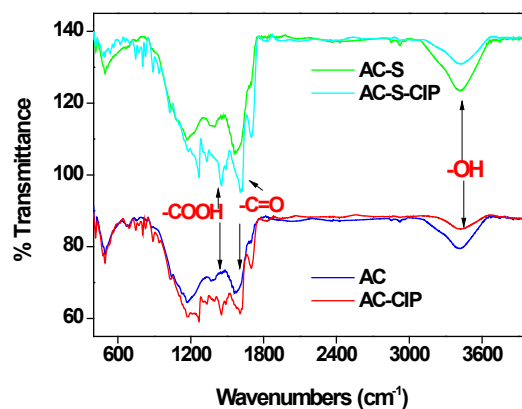


Fig. 3. Fourier transform infrared spectra of AC, AC-CIP, and AC-S, AC-S-CIP.

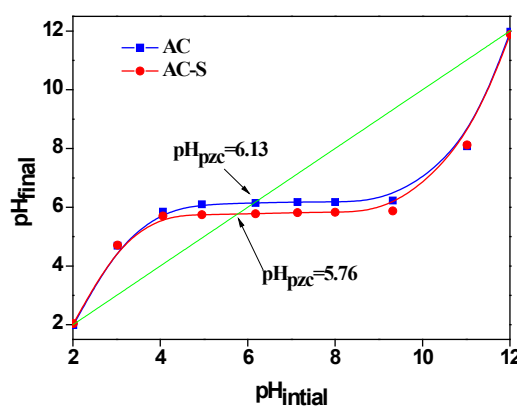


Fig. 4. The points of zero charge (PZC) onto AC and AC-S.

activated carbons were protonated with a positive charge, whereas in $\text{pH} > \text{pH}_{\text{pzc}}$, adsorbents were deprotonated with a negative charge. Carabineiro et al. [37] demonstrated that activated carbons with more acid groups and oxygen-containing groups constantly showed lower pH_{pzc} , accounting for lower pH_{pzc} of AC-S than AC. AC-S yielded more total acid groups, which significantly influenced adsorption of CIP, as discussed in Section 3.4.

3.2. Adsorption kinetic

Three kinetic models, pseudo-first-order, pseudo second-order, and intraparticle diffusion were applied to fit experimental data to analyze adsorption kinetics.

The pseudo-first-order kinetic model is expressed as follows:

$$Q_t = Q_e (1 - e^{-k_1 t}) \quad (3)$$

where Q_e and Q_t correspond to amounts of CIP adsorbed at equilibrium and at time t (min), respectively; and k_1 (min^{-1}) represents constant rate of the pseudo-first-order model.

The pseudo-second-order kinetic model is represented as follows:

$$\frac{t}{Q_t} = \frac{1}{k_2 Q_e^2} + \frac{t}{Q_e} \quad (4)$$

where k_2 ($\text{g}/\text{mg min}$) refers to constant rate of pseudo-second-order adsorption.

Intraparticle diffusion model is expressed as follows:

$$Q_t = k_{\text{dif}} t^{1/2} + C \quad (5)$$

where k_{dif} ($\text{mg}/\text{g min}^{-1/2}$) stands for intraparticle diffusion rate constant; and C represents thickness of boundary layer.

Fig. 5 displays results. Rapid adsorption was caused by hydrophobic interaction between pollutant and adsorbent in water. During the first 130 min, adsorption capacity of AC increased faster than AC-S. This phenomenon can be explained by faster physical adsorption in comparison with chemical adsorption. According to Fig. 5, adsorption

rate of AC was higher than that of AC-S. Specifically, AC reached adsorption saturation within 300 min, with maximum adsorption capacity of 323.70 mg/g. Conversely, AC-S required more time to saturate, whereas its adsorption capacity (407.75 mg/g) was much higher than that of AC. This result can be attributed to more adsorption sites present on adsorbents, resulting in CIP adsorption on external carbon surface. With processing of adsorption, available adsorption sites on external surface significantly lessened, and thus, CIP required more time to diffuse and adsorb on the internal surface. As such, adsorption became difficult as the number of vacant sites decreased, and a repulsive force formed between solute molecules on solid surface and in bulk phase [34]. Another probable reason was that AC-S featured more acid groups, which resulted in time-dependent adsorption capacity. This result suggested that at the initial stage, adsorption was controlled by physical adsorption, whereas chemical adsorption dominated the latter stage. Time for adsorption equilibrium was also related to initial concentration of CIP [38].

Intraparticle diffusion model based on the Weber and Morris theory can reflect linear regression between Q_t versus $t^{1/2}$ and intercept C . Zero value of C indicates that adsorption is controlled only by intraparticle diffusion. In this process, regression was linear with non-zero C value, suggesting that adsorption followed intraparticle diffusion in addition to pseudo-second-order kinetic model. Similarly, C values can provide insights into thickness of boundary layer. Higher intercept led to more significant boundary layer effect [39]. Intraparticle diffusion equation was used to analyze CIP adsorption by activated carbon in three stages: the initial stage, which was attributed to rapid external diffusion and surface adsorption; gradual adsorption stage, where intraparticle diffusion represented the rate limiting step; and the third region, which was the final equilibrium stage, in which intraparticle diffusion decelerated due to extremely low pollutant concentration. Accordingly, both surface adsorption and intraparticle diffusion affected AC and AC-S adsorption on CIP (Table 3).

Table 3 lists all kinetic parameters and correlation coefficients. Maximum adsorption capacities of AC and AC-S measured 323.70 and 407.75 mg/g, respectively. The criterion for applicability of these models was based on respective correlation coefficient (R^2) and agreement between experimental and calculated value of Q_e . Compared with pseudo-first-order and intraparticle diffusion, the pseudo-second-order model proved to be a better fit for AC and AC-S with higher R^2 value (>0.999). Maximum adsorption capacity obtained from experiments was similar to the value obtained using the pseudo-second-order kinetic model. Carabineiro et al. [29] reported similar experimental results, in which the pseudo-second-order kinetic model was considered more suitable for CIP adsorption on adsorbent from aqueous solution.

3.3. Adsorption isotherms

Three isotherms, namely, the Langmuir, Freundlich, and Tempkin isotherms, were applied to analyze sorption of AC and AC-S. Fig. 6 displays adsorption ability of CIP on activated carbon. With increase in CIP concentration, mass transfer pressure of adsorption within adsorbents

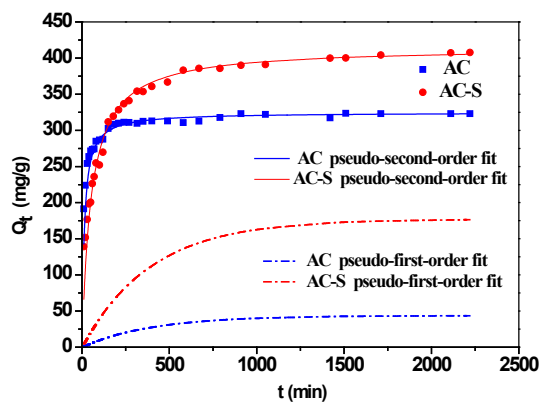


Fig. 5. Adsorption kinetics fitted by pseudo-first order and pseudo-second-order models ($C_0 = 200$ mg/L; carbon dosage = 0.4 g/L; $\text{pH} = 6.04$; temperature = $30 \pm 1^\circ\text{C}$).

Table 3
Parameters of kinetics models for CIP adsorption

| Kinetic models | Parameters | AC | AC-S | | |
|-------------------------|---|----------------------|----------------------|--------------|--------|
| Pseudo-first-order | k_1 (1/min) | 2.5×10^{-3} | 2.5×10^{-3} | | |
| | Q_{cal} (mg/g) | 43.63 | 176.93 | | |
| | R^2 | 0.6535 | 0.9426 | | |
| Pseudo-second-order | k_2 (1/min) | 2×10^{-4} | 4×10^{-5} | | |
| | Q_{cal} (mg/g) | 324.68 | 414.94 | | |
| | V_0 (mg/(g min)) | 25.62 | 7.92 | | |
| | R^2 | 0.9999 | 0.9997 | | |
| Intraparticle diffusion | k_{dif} (mg/(g min ^{-1/2})) | 13.29 | 17.99 | First stage | |
| | | C | 167.38 | | 80.14 |
| | | R^2 | 0.8551 | | 0.9666 |
| | k_{dif} (mg/(g min ^{-1/2})) | 1.63 | 5.79 | Second stage | |
| | | C | 281.63 | | 244.51 |
| | | R^2 | 0.5054 | | 0.9547 |
| | k_{dif} (mg/(g min ^{-1/2})) | 0.48 | 1.13 | Third stage | |
| | | C | 304.70 | | 355.69 |
| | | R^2 | 0.4848 | | 0.9819 |
| | Q_{exp} (mg/g) | | 323.10 | 407.75 | |

$C_0 = 200$ mg/L; Carbon dosage = 0.4 g/L; pH = 6.04.

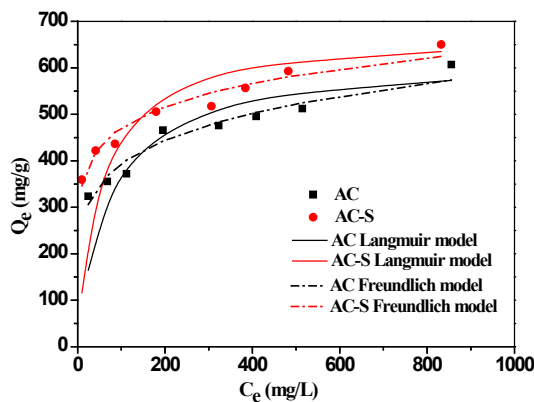


Fig. 6. Sorption isotherms of CIP for AC and AC-S fitted by Langmuir model (solid lines) and Freundlich model (dash lines) ($C_0 = 200$ mg/g; carbon dose = 0.4 g/L; pH = 6.04; temperature = $30 \pm 1^\circ\text{C}$).

increased. Increasing pressure enhanced internal diffusion of activated carbons, thereby increasing adsorption capacity. Adsorption isotherms described the interaction between CIP and adsorbents. As shown in Table 4, adsorption of CIP onto AC and AC-S fit well the Langmuir isotherm model with highest values of R^2 (0.9818, 0.98509, respectively) among all isotherms. According to the Langmuir isotherm [40], adsorption was uniform, and each site only accepted one CIP molecule without further adsorption at that site. The Langmuir isotherm is used for monolayer adsorption on specific homogenous sites with finite number of identical sites. The linear equation is given by:

$$\frac{C_e}{Q_e} = \frac{1}{Q_{max}} C_e + \frac{1}{K_L Q_{max}} \quad (6)$$

where Q_e (mg/g) represents the amount of adsorbate adsorbed per unit mass of adsorbent at equilibrium; C_e (mg/L) corresponds to equilibrium concentration at different initial concentrations; Q_{max} (mg/g) refers to maximum adsorption capacity; K_L (L/mol) stands for Langmuir constant, which indicates adsorption rate; and R_L is an essential feature of Langmuir isotherm, which is defined by the following:

$$R_L = \frac{1}{1 + bC_0} \quad (7)$$

where C_0 (mg/L) corresponds to initial concentration of CIP; R_L refers to isotherms that can be irreversible ($R_L = 0$), favorable ($0 < R_L < 1$), linear ($R_L = 1$), or unfavorable ($R_L > 1$).

Based on the linear form of Langmuir isotherm model (Table 4), values of K_L and Q_{max} were obtained from the intercept and slope of the plot of C_e/q_e versus C_e , respectively. Results showed that adsorption favored AC and AC-S. Calculated R_L was between 0 and 1, indicating preferential adsorption of CIP on activated carbon. The value for CIP adsorption onto AC-S was slightly lower than that of AC, indicating that modification of AC-S improved adsorption.

The Freundlich [41] isotherm is an empirical equation with no assumptions. The linear equation is as follows:

$$\ln Q_e = \ln K_F + \frac{1}{n} \ln C_e \quad (8)$$

where K_F (L/mol) is the Freundlich constant.

Parameters of Freundlich isotherm model include K_F and $1/n$ (capacity and intensity of adsorption); they were calculated from the intercept and slope of the linear plot of $\ln Q_e$ versus $\ln C_e$, respectively. The value of $1/n$ indicates effect of concentration on adsorption capacity. Usually, a smaller $1/n$ value indicates better adsorption of activated carbon. When $1/n$ lies between 0.1 and 0.5, activated carbon is easily adsorbed; when $1/n > 2$, activated carbon is difficult to adsorb. As shown in Table 5, $1/n$ values of AC and AC-S reached 0.18 and 0.13 respectively, revealing favorable adsorption in both experiments.

The Tempkin [42] isotherm relates adsorbents and adsorbate; heat of adsorption decreases throughout adsorption. The equation is as follows:

$$Q_e = B \ln K_T + B \ln C_e \quad (9)$$

$$B = RT/b \quad (10)$$

where K_T represents the equilibrium binding constant; R (8.314 J/mol K) refers to the universal gas constant; and T (K) is absolute solution temperature.

The Langmuir isotherm was the most suitable isotherm. In Langmuir isotherm fitting, R^2 values approximately reached 1, which was higher than R^2 values calculated using the other two isotherms. Observed k_L values showed that adsorbent preferred binding acidic ions and that speciation predominated on sorbent characteristics when ion exchange was the predominant mechanism in adsorption

Table 4
Constants of adsorption isotherms for CIP adsorption

| Isotherm models | Constants | AC | AC-S |
|-----------------|------------------------------------|-----------|-----------|
| Langmuir | Q_m (mg/g) | 617.28 | 671.14 |
| | b (L/mg) | 0.0151 | 0.0213 |
| | R_L | 0.06–0.30 | 0.01–0.23 |
| | R^2 | 0.9818 | 0.9851 |
| Freundlich | K_F (mg/g) (L/mg) ^{1/n} | 175.19 | 255.84 |
| | 1/n | 0.18 | 0.13 |
| | R^2 | 0.9376 | 0.9485 |
| Tempkin | K_T | 1.8218 | 2.0404 |
| | B | 33.9334 | 40.3427 |
| | R^2 | 0.9027 | 0.8995 |

of CIP. Results also suggested that Langmuir isotherm was more suitable for characterizing adsorption of activated carbon under different initial concentrations of CIP. Monolayer adsorption was observed in this study.

3.4. Effect of ionic strength on CIP adsorption

Wastewater with antibiotics often contains various salts, which lead to high ionic strength that affect adsorption. Adsorption experiments evaluated effects of ionic strength with various salts in wastewater. Fig. 7a presents CIP adsorption data on water with different ionic strengths (0.1 and 0.5 mol/L as NaCl). As shown in Fig. 7a, the amount of adsorbed CIP changed slightly with increase in NaCl concentration, indicating that ionic strength hardly affected CIP adsorption. Maximum adsorption capacities of AC and AC-S measured 362.64 and 406.91 mg/g at NaCl concentration of 0.1 mol/L, respectively. Given that AC-S was not affected by salinity in the test, this type of activated carbon may be widely used in industrial wastewater for CIP adsorption.

3.5. Effect of solution pH on adsorption

Previous studies reported that solution pH plays a significant role in adsorption of activated carbon [43]. Fig. 7b shows effect of solution pH on adsorption. In the tested pH range (from pH 2 to pH 7), AC and AC-S exhibited pH-dependent CIP adsorption. As previously mentioned, pH_{pzc} of AC and AC-S reached 6.13 and 5.16, respectively, and were negatively charged. Among all pH values included in experiments, pH_{pzc} was related to contents of surface groups. When pH of solution reached below 6.1 (pK_{a1}), CIP^+ was the main component in solution due to protonation of the amine group. When pH value fell between 6.1 and 8.7 (pK_{a2}), CIP^0 served as primary component of solution. When pH of solution measured above 8.7, CIP^- dominated the solution. Charge on activated carbon surface was converted from positive to negative as initial pH increased from 2 to 7. Therefore, at low pH values (2–4.5), electrostatic repulsion occurred between activated carbons and CIP. Competition between CIP^+ and H^+ for adsorption sites on activated carbon possibly resulted in lower adsorption capacity in comparison with that at higher pH conditions. When solution

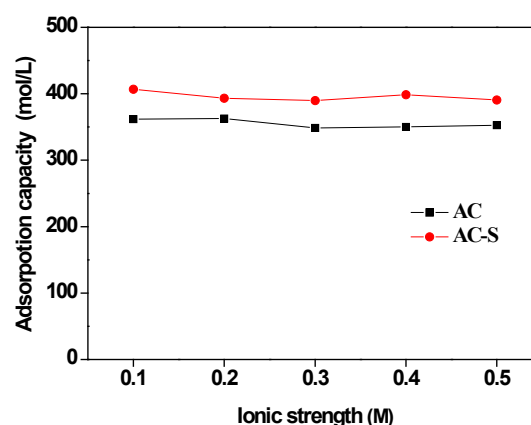


Fig. 7. Effect of NaCl on the adsorption of CIP by AC and AC-S ($C_0 = 200$ mg/g; carbon dose = 0.4 g/L; temperature = $30 \pm 1^\circ C$).

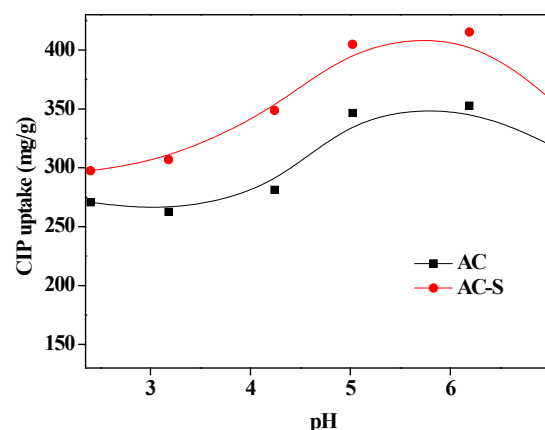


Fig. 8. Effect of initial pH on the removal of CIP by AC and AC-S ($C_0 = 200$ mg/g; carbon dose = 0.4 g/L; temperature = $30 \pm 1^\circ C$).

pH was between 5 and 6.1, electrostatic attraction between adsorbent and CIP^0 dominated, and mechanism of CIP removal from solution was partly cationic exchange. As pH increased, electrostatic interaction probably weakened, as hydrophobic interaction was enhanced. Under optimum condition of pH 5.77, adsorption capacities reached 349.35 and 407.09 mg/g for AC and AC-S, respectively.

When $pH > 7.5$ [44], CIP precipitates, and adsorption capacity is overestimated. As such, only pH values ranging from 2 to 7 were considered in this study. Fallati et al. [45] reported that CIP features different solubilities under different pH values, and maximum solubility of initial CIP concentration measured 110 mg/L at $pH = 7.5$. This result showed lower affinity to activated carbon. This study avoided using pH value at 7.5, at which CIP^0 is in the highest concentration, and CIP features the lowest affinity. In polar solvents, CIP solubility decreases with formation of intramolecular hydrogen bonds between molecules of the compound.

CIP adsorption onto AC and AC-S involved strong interactions between CIP in water and surface groups in molecular structure. Given the numerous electronic sites, CIP can be easily protonated [30]. Amino group is a

Table 5
Comparison of CIP adsorption capacity by different carbon

| Activated source carbon | S_{BET} (m^2/g) | $S_{\text{mic}}/S_{\text{BET}}$ (%) | (mg/g) | Experimental conditions | | | | Modification | Reference |
|-------------------------------|---|--|--------|-------------------------|-------------------------|-----------------------|----------------------------------|--------------|------------|
| | | | | pH | T($^{\circ}\text{C}$) | Adsorbent dosage(g/L) | Initial CIP concentration (mg/L) | | |
| Palm leaves | 24.4 | – | 40.02 | 6 | 25 | 0.4 | 100 | | [9] |
| <i>Arundodonax Linn</i> | 1568 | 55.8 | 300.00 | 6.0 | 25 | 1 | 400 | | [37] |
| porous resins MN-150 | 815.3 | 46.9 | 80.00 | 5.5 | 30 | 0.34 | 100 | | [38] |
| porous resins MN-202 | 1155.8 | 60.3 | 99.88 | 5.5 | 30 | 0.34 | 100 | | [38] |
| carbon xerogel | 617.0 | 0.0 | 80.02 | 6.5 | 25 | 0.05 | 10 | | [20] |
| carbon nanotubes | 284.0 | 0.0 | 100.00 | 5 | 25 | 0.05 | 10 | | [20] |
| corn stalk | 1091.2 | 53.5 | 323.10 | 5.76 | 30 | 0.4 | 200 | no | This study |
| silage pre-treated corn stalk | 741.6 | 78.2 | 407.75 | 6.04 | 30 | 0.4 | 200 | no | This study |

stronger electron-donating group than $-\text{OH}$ [46]. Amino groups of CIP molecules can be positively charged under acidic conditions and achieve electronic coupling [30]. CIP features a benzene ring and two heterocyclic rings. However, fluorine in the benzene ring, with its strong electronic adsorption ability, can easily provide electron vacancies in the benzene ring as π -electron acceptors. The rich electronic region, which can be used as π -electron donor via π - π EDA interaction, can cause extremely strong adsorption in activated carbon [47].

Amino groups of CIP molecules can be protonated by H^+ in solution, whereas some acid groups of AC and more acid groups of AC-S can be deprotonated by silage pretreatment. AC-S contained more acid groups, contributing to stronger adsorption capacity of AC-S than AC.

3.6. Comparison of characteristics

Table 5 lists adsorption capacities and other characteristics of CIP on different adsorbents. The activated carbon prepared in this work (AC-S) showed the highest adsorption capacity (407.75 mg/g) compared with those prepared from palm leaves and *Arundo donax Linn*. For AC-S, the proportion of micropore volume in specific surface area was significantly high, and appearance of micropores in other activated carbons was far less than this proportion. AC-S was more efficient in terms of adsorption of CIP. AC-S is also more cost-effective as modifying agents are not needed during modification. Therefore, modifying activated carbon developed from corn stalks with novel silage pre-treatment is a promising approach for treatment of CIP in wastewater.

4. Conclusions

This study proposed a novel silage pre-treatment method for developing activated carbon from corn stalks. AC-S presented more micropores and irregular surface compared with ACs. Adsorption capacity of CIP by AC-S increased, and equilibrium data were more suitable for Langmuir and pseudo-second-order models. Batch experiments revealed that adsorption capacity of CIP increased with increasing initial concentration, contact time, and pH

values. Adsorption mechanisms include hydrophobic interaction, chemical adsorption, electrostatic attraction, and π - π EDA interaction.

Acknowledgments

We gratefully acknowledge financial support by the Natural Science Foundation of Shandong Province (ZR2016DB13), the National Natural Science Foundation of China (21307078), one sub-subject of the Major Projects of National Science and Technology (2012ZX07404-003-006), the National the Foundation of Co-innovation Center of Green Building of Shandong Province (LSXT201507), and Key Research and Development Projects in Shandong Province (2015GSF122007).

References

- [1] W. Li, Y. Shi, L. Gao, J. Liu, Y. Cai, Occurrence, distribution and potential affecting factors of antibiotics in sewage sludge of wastewater treatment plants in China, *Sci. Total Environ.*, 445 (2013) 306–313.
- [2] Y. Tan, Y. Guo, X. Gu, C. Gu, Effects of metal cations and fulvic acid on the adsorption of ciprofloxacin onto goethite, *Environ. Sci. Pollut. Res.*, 22 (2015) 609–617.
- [3] X. He, Z. Wang, X. Nie, Y. Yang, D. Pan, A.O. Leung, Z. Cheng, Y. Yang, K. Li, K. Chen, Residues of fluoroquinolones in marine aquaculture environment of the Pearl River Delta, South China, *Environ. Geochem. Health*, 34 (2012) 323–335.
- [4] Y. Picó, V. Andreu, Fluoroquinolones in soil—risks and challenges, *Anal. Bioanal. Chem.*, 387 (2007) 1287–1299.
- [5] X. Peng, F. Hu, F.L. Lam, Y. Wang, Z. Liu, H. Dai, Adsorption behavior and mechanisms of ciprofloxacin from aqueous solution by ordered mesoporous carbon and bamboo-based carbon, *J. Colloid Interface Sci.*, 460 (2015) 349–360.
- [6] X. Peng, K. Zhang, C. Tang, Q. Huang, Y. Yu, J. Cui, Distribution pattern, behavior, and fate of antibacterials in urban aquatic environments in South China, *J. Environ. Monit.*, 13 (2011) 446–454.
- [7] R. Zhang, G. Zhang, Q. Zheng, J. Tang, Y. Chen, W. Xu, Y. Zou, X. Chen, Occurrence and risks of antibiotics in the Laizhou Bay, China: impacts of river discharge, *Ecotoxicol. Environ. Saf.*, 80 (2012) 208–215.
- [8] H. Chen, B. Gao, H. Li, Removal of sulfamethoxazole and ciprofloxacin from aqueous solutions by graphene oxide, *J. Hazard. Mater.*, 282 (2015) 201–207.

- [9] E.-S.I. El-Shafey, H. Al-Lawati, A.S. Al-Sumri, Ciprofloxacin adsorption from aqueous solution onto chemically prepared carbon from date palm leaflets, *J. Environ. Sci.*, 24 (2012) 1579–1586.
- [10] Y. Wang, H. Ngo, W. Guo, Preparation of a specific bamboo based activated carbon and its application for ciprofloxacin removal, *Sci. Total Environ.*, 533 (2015) 32–39.
- [11] Y. Sun, Q. Yue, B. Gao, L. Huang, X. Xu, Q. Li, Comparative study on characterization and adsorption properties of activated carbons with H_3PO_4 and $H_2P_2O_7$ activation employing *Cyperus alternifolius* as precursor, *Chem. Eng. J.*, 181 (2012) 790–797.
- [12] Y. Kang, Z. Guo, J. Zhang, H. Xie, H. Liu, C. Zhang, Enhancement of Ni (II) removal by urea-modified activated carbon derived from *Pennisetum alopecuroides* with phosphoric acid activation, *J. Taiwan Inst. Chem. Eng.*, 60 (2016) 335–341.
- [13] H. Liu, Q. Gao, P. Dai, J. Zhang, C. Zhang, N. Bao, Preparation and characterization of activated carbon from lotus stalk with guanidine phosphate activation: sorption of Cd (II), *J. Anal. Appl. Pyrolysis*, 102 (2013) 7–15.
- [14] Z. Guo, J. Zhang, H. Liu, Ultrahigh Rhodamin B adsorption capacities from aqueous solution by activated carbon derived from *Phragmites australis* doped with organic acid by phosphoric acid activation, *RSC Adv.*, 47 (2016) 40818–40827.
- [15] L. Zheng, Z. Dang, X. Yi, H. Zhang, Equilibrium and kinetic studies of adsorption of Cd (II) from aqueous solution using modified corn stalk, *J. Hazard. Mater.*, 176 (2010) 650–656.
- [16] A. Bakar, A. Ashrif, N.S. Hassan, The effectiveness of corn cob activated carbon in rainwater harvesting filtration system, in: *Technology, Informatics, Management, Engineering, and Environment (TIME-E)*, 2014 2nd International Conference on, IEEE, 2014, pp. 86–89.
- [17] L. Zheng, Z. Dang, C. Zhu, X. Yi, H. Zhang, C. Liu, Removal of cadmium(II) from aqueous solution by corn stalk graft copolymers, *Bioresour. Technol.*, 101 (2010) 5820.
- [18] S. Chen, Q. Yue, B. Gao, Q. Li, X. Xu, Removal of Cr (VI) from aqueous solution using modified corn stalks: Characteristic, equilibrium, kinetic and thermodynamic study, *Chem. Eng. J.*, 168 (2011) 909–917.
- [19] M.R. Fathi, A. Asfaram, A. Farhangi, Removal of Direct Red 23 from aqueous solution using corn stalks: isotherms, kinetics and thermodynamic studies, *Spectrochim. Acta, Part.*, (2015) 364–372.
- [20] S. Li, L. Sun, L. Wang, Y. Wang, Preparation and electrochemical performance of corn straw-based nanoporous carbon, *J. Porous Mater.*, 22 (2015) 1351–1355.
- [21] P.A. Gerin, F. Vliegen, J.-M. Jossart, Energy and CO_2 balance of maize and grass as energy crops for anaerobic digestion, *Bioresour. Technol.*, 99 (2008) 2620–2627.
- [22] S. Weiß, A. Zankel, M. Leubhn, S. Petrak, W. Somitsch, G. Guebitz, Investigation of microorganisms colonising activated zeolites during anaerobic biogas production from grass silage, *Bioresour. Technol.*, 102 (2011) 4353–4359.
- [23] H. Pobeheim, B. Munk, H. Lindorfer, G.M. Guebitz, Impact of nickel and cobalt on biogas production and process stability during semi-continuous anaerobic fermentation of a model substrate for maize silage, *Water Res.*, 45 (2011) 781–787.
- [24] H. Boehm, Chemical Identification of Surface Groups, *Adv. Catal.*, (1966) 179–274.
- [25] M. Kosmulski, The pH dependent surface charging and points of zero charge. VI. Update, *J. Colloid Interface Sci.*, 426 (2014) 209–212.
- [26] F. Ansari, M. Ghaedi, M. Taghdiri, A. Asfaram, Application of ZnO nanorods loaded on activated carbon for ultrasonic assisted dyes removal: Experimental design and derivative spectrophotometry method, *Ultrason. Sonochem.*, 33 (2016) 197–209.
- [27] M. Roosta, M. Ghaedi, A. Asfaram, Simultaneous ultrasonic-assisted removal of malachite green and safranin O by copper nanowires loaded on activated carbon: central composite design optimization, *Rsc Adv.*, 5 (2015) 57021–57029.
- [28] M. Donohue, G. Aranovich, Classification of Gibbs adsorption isotherms, *Adv. Colloid Inter. Sci.*, 76 (1998) 137–152.
- [29] S. Carabineiro, T. Thavorn-Amornsri, M. Pereira, P. Serp, J. Figueiredo, Comparison between activated carbon, carbon xerogel and carbon nanotubes for the adsorption of the antibiotic ciprofloxacin, *Catal. Today*, 186 (2012) 29–34.
- [30] H. Liu, J. Zhang, H.H. Ngo, W. Guo, H. Wu, Z. Guo, C. Cheng, C. Zhang, Effect on physical and chemical characteristics of activated carbon on adsorption of trimethoprim: mechanisms study, *RSC Adv.*, (2015) 85187–85195.
- [31] N. Yoshizawa, K. Maruyama, Y. Yamada, M. Zielinska-Blajet, XRD evaluation of CO_2 activation process of coal-and coconut shell-based carbons, *Fuel*, 79 (2000) 1461–1466.
- [32] G. Fang, H. Li, Z. Chen, X. Liu, Preparation and characterization of stearic acid/expanded graphite composites as thermal energy storage materials, *Energy*, 35 (2010) 4622–4626.
- [33] Y. Juan, Q. Ke-Qiang, Preparation of activated carbon by chemical activation under vacuum, *Environ. Sci. Technol.*, 43 (2009) 3385–3390.
- [34] S. Min, J. Han, E. Shin, J. Park, Improvement of cadmium ion removal by base treatment of juniper fiber, *Water Res.*, 38 (2004) 1289–1295.
- [35] A. Asfaram, M. Ghaedi, G.R. Ghezalbash, Biosorption of Zn^{2+} , Ni^{2+} and Co^{2+} from water samples onto *Yarrowia lipolytica* ISF7 using a response surface methodology, and analyzed by inductively coupled plasma optical emission spectrometry (ICP-OES), *Rsc Adv.*, 6 (2016) 23599–23610.
- [36] H. Liu, X. Wang, G. Zhai, J. Zhang, C. Zhang, N. Bao, C. Cheng, Preparation of activated carbon from lotus stalks with the mixture of phosphoric acid and pentaerythritol impregnation and its application for Ni (II) sorption, *Chem. Eng. J.*, 209 (2012) 155–162.
- [37] S. Carabineiro, T. Thavorn-Amornsri, M. Pereira, J. Figueiredo, Adsorption of ciprofloxacin on surface-modified carbon materials, *Water Res.*, 45 (2011) 4583–4591.
- [38] H. Mazaheri, M. Ghaedi, A. Asfaram, S. Hajati, Performance of CuS nanoparticle loaded on activated carbon in the adsorption of methylene blue and bromophenol blue dyes in binary aqueous solutions: Using ultrasound power and optimization by central composite design, *J. Mol. Liq.*, 219 (2016) 667–676.
- [39] A. Asfaram, M. Ghaedi, S. Hajati, A. Goudarzi, E.A. Dil, Screening and optimization of highly effective ultrasound-assisted simultaneous adsorption of cationic dyes onto Mn-doped Fe_3O_4 -nanoparticle-loaded activated carbon, *Ultrason. Sonochem.*, 34 (2017) 1–12.
- [40] S. Agarwal, I. Tyagi, V.K. Gupta, A.R. Bagheri, M. Ghaedi, A. Asfaram, S. Hajati, A.A. Bazrafshan, Rapid adsorption of ternary dye pollutants onto copper (I) oxide nanoparticle loaded on activated carbon: Experimental optimization via response surface methodology, *J. Environ. Chem. Eng.*, 4 (2016) 1769–1779.
- [41] M. Ghaedi, E. Barakat, S. Hajati, A. Asfaram, A. Bazrafshan, Efficient adsorption of Europtal on activated carbon modified with ligands (1E, 2E)-1,2-bis (pyridin-4-ylmethylene) hydrazine (M) and (1E, 2E)-1,2-bis (pyridin-3-ylmethylene) hydrazine (SCH-4); Response surface methodology, *Rsc Advances*, 5 (2015) 42376–42387.
- [42] M. Temkin, V. Pyzhev, Kinetics of ammonia synthesis on promoted iron catalysts, *Acta physiochim. URSS*, 12 (1940) 217–222.
- [43] H. Demiral, G. Gündüzoğlu, Removal of nitrate from aqueous solutions by activated carbon prepared from sugar beet bagasse, *Bioresour. Technol.*, 101 (2010) 1675–1680.
- [44] M.E.R. Jalil, M. Baschini, K. Sapag, Influence of pH and antibiotic solubility on the removal of ciprofloxacin from aqueous media using montmorillonite, *Appl. Clay Sci.*, 114 (2015) 69–76.
- [45] C. Fallati, A. Ahumada, R. Manzo, El perfil de solubilidad de la ciprofloxacina en función del pH, *Acta Farm. Bonaerense*, 13 (1994) 73–77.
- [46] D.P. Pursell, Adapting to student learning styles: Engaging students with cell phone technology in organic chemistry instruction, *J. Chem. Educ.*, 86 (2009) 1219.
- [47] W. Chen, L. Duan, D. Zhu, Adsorption of hydroxyl- and amino-substituted aromatics to carbon nanotubes, *Environ. Sci. Technol.*, 42 (2008) 6862–6868.